Electronic Supporting Information for

A New Iron-Based Metal–Organic Framework with Enhancing Catalysis Activity for Benzene Hydroxylation

Thach N. Tu,[*,a,b] Hue T. T. Nguyen,[b,c] Huong T. D. Nguyen,[c] My V. Nguyen,[c] Trinh D. Nguyen,[a] Nhung T. Tran,[d] Kwon T. Lim[e]

[a]Nguyen Tat Thanh University, 300A Nguyen Tat Thanh Street, District 4, Ho Chi Minh City 755414, Vietnam.
[b]Center for Innovative Materials and Architectures (INOMAR), Vietnam National University-Ho Chi Minh (VNU-HCM), Ho Chi Minh City 721337, Vietnam.
[c]University of Science, Vietnam National University-Ho Chi Minh (VNU-HCM), Ho Chi Minh City 721337, Vietnam.
[d]Ho Chi Minh City University of Technology and Education (HCMUTE), 01 Vo Van Ngan Street, Thu Duc District, Ho Chi Minh City 720100, Vietnam.
[e]Department of Display Engineering, Pukyong National University, Busan, 608-737, South Korea.

Table of Contents

Section S1 Materials and Analytical Techniques

Analytical Techniques. Thermal gravimetric analysis (TGA) was performed using a TA Q500 thermal analysis system under air flow. Fourier transform infrared (FT-IR) spectra were recorded on a Bruker Vertex 70 spectrometer using the attenuated total reflectance (ATR) sampling method. N_2 adsorption measurements were performed using a Micromeritics 3Flex Surface Characterization Analyzer. A liquid N_2 bath was used for the measurement at 77 K. Elemental analysis was performed using a LECO CHNS-932 analyzer. The gas chromatography (GC, model: Agilent System 19091s-433) equipped with a flame ionization detector (FID) was used to determine the yield of catalytic reactions. Toluene was used as an internal standard to quantify the yield of catalytic reactions.

The theoretical prediction of surface area by Materials studio 8.0. The surface area of Fe-TBAPy was calculated using the “Atom Volumes & surfaces” tool in Materials studio 8.0 (menu Tools / Atom Volumes & surfaces) with the solvent radius, which is equal to that of N_2 kinetic radius (1.82 Å), was chosen. The accessible solvent surface for one unit cell was then shown in the analysis tab and surface area of Fe-TBAPy could be calculated by converting the above value to the surface area per one gram of Fe-TBAPy.

Powder X-ray Diffraction Analysis and structure solution. Powder X-ray data were collected using a Bruker D8 Advance employing Ni-filtered Cu Kα (λ = 1.54178 Å). The system was equipped with an anti-scattering shield that prevents incident diffuse radiation from hitting the detector.

Section S2 Reaction Scheme and Microscope Image of Fe-TBAPy

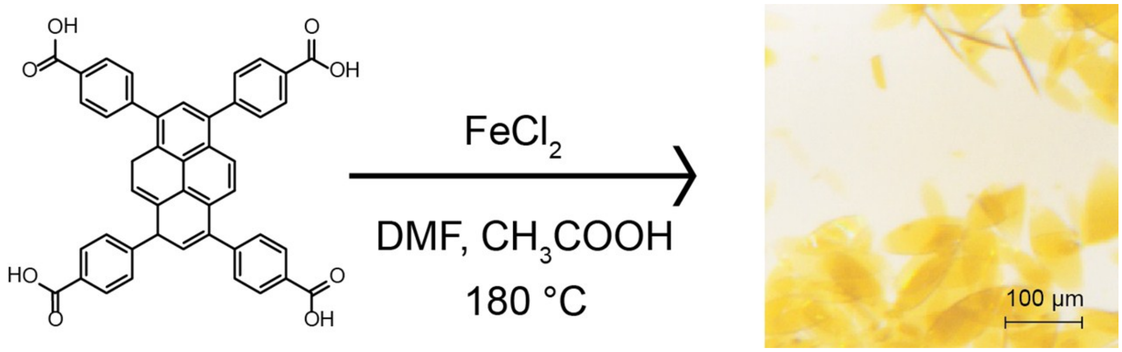

Figure S1. Reaction scheme and microscope image of Fe-TBAPy crystals.

Section S3 Powder X-ray Diffraction Patterns

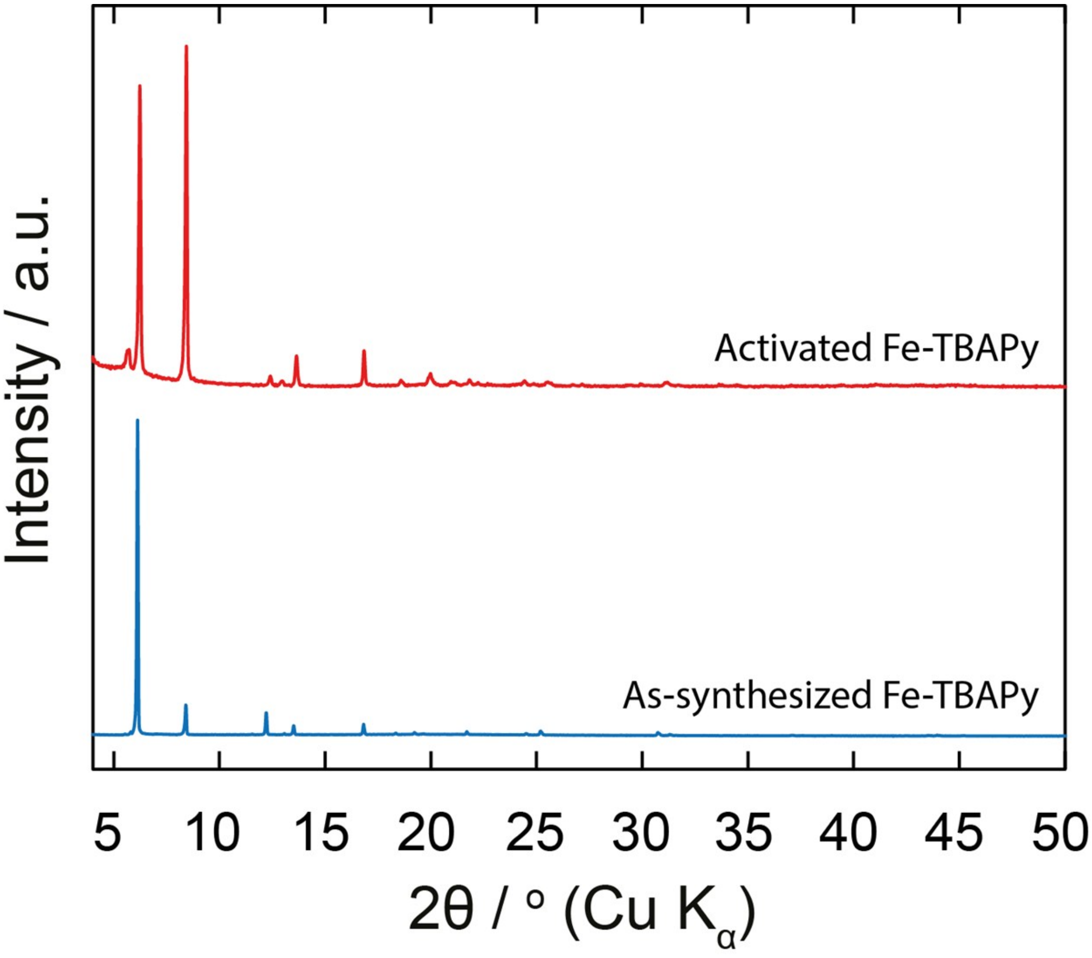

Figure S2. Powder X-ray diffraction patterns of the as-synthesized and activated Fe-TBAPy.

Section S4 Structural Solution of Fe-TBAPy

Determination of unit cell parameters. The diffraction data for activated Fe-TBAPy was analyzed by the program Materials Studio ver. 8.0, Accelrys Software Inc (pattern indexing and Pawley refinement). The unit cell length (a = 14.2972; b = 15.5453; c = 14.0069 Å; $\alpha = \gamma = 90$ and $\beta = 84.79$ °) was determined by Pawley refinements. The Bravais lattice of Fe-TBAPy is determined to adopt the monoclinic system with *P2/c* space group (No. 13).

Structural Modeling of Fe-TBAPy. The modeled framework with the atomic connectivity, which is similar to the compound toluene@[$In_2(OH)_2$(TBAPy)],[1] was built using the Materials Visualizer module of Materials Studio ver. 8.0 software. Subsequently, the full profile pattern fitting (Rietveld method) was performed against the experimental powder pattern of Fe-TBAPy with 2θ = 2° – 80°. This showed a satisfactory result with the fitting that converged at reasonable residual values (Rwp = 9.92%, Rp = 7.53%). The final unit cell parameters (a = 14.2972; b = 15.5453; c = 14.0069 Å; $\alpha = \gamma = 90$ and $\beta = 84.79$ °), the fractional atomic coordinates and crystal structure information of Fe-TBAPy after the Rietveld refinement are presented in Table S1.

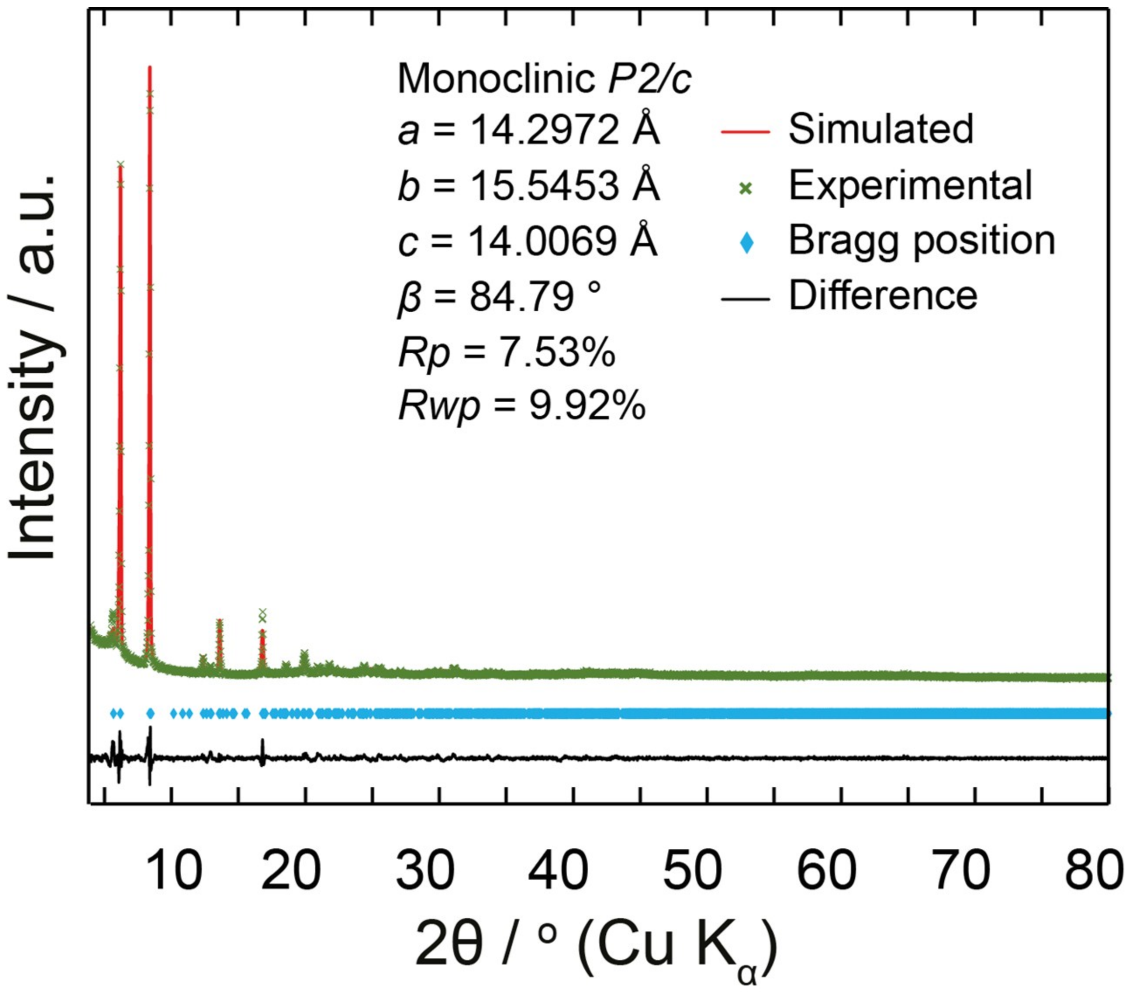

Figure S3. Full range Rietveld refined PXRD patterns of activated Fe-TBAPy.

Table S1. Atomic coordinates and refined unit cell parameters of Fe-TBAPy.

Name	**Fe-TBAPy**			
Space group	*P2/c*			
a	14.2972 Å			
b	15.5453 Å			
c	14.0069 Å			
β	84.79 °			
R_p	7.53%			
R_wp	9.92%			
Atom Name	*x*	*y*	*z*	Site Occupancy
Fe1	0.5	0	0	1
Fe2	0.5	0.0082	0.25	1
C1	0.3896	0.8813	0.1587	1
C2	0.3897	0.1225	0.1652	1
C3	0.32621	0.81833	0.17772	1
C4	0.32864	0.1916	0.17985	1
C5	0.31525	0.77086	0.25636	1
C6	0.31437	0.23608	0.25969	1
C7	0.2695	0.6955	0.2648	1
C8	0.2692	0.3118	0.2667	1
C9	0.2313	0.6656	0.1945	1
C10	0.2318	0.3411	0.1954	1
C11	0.23418	0.71864	0.12149	1
C12	0.2367	0.2876	0.1212	1
C13	0.28365	0.79313	0.11167	1
C14	0.2855	0.21309	0.11281	1
C15	0.1814	0.5813	0.2031	1
C16	0.1815	0.4256	0.2024	1
C17	0.0895	0.5824	0.2261	1
C18	0.0896	0.4245	0.2264	1
C19	0.0483	0.6641	0.2312	1
C20	0.0484	0.343	0.2306	1
C21	0.2297	0.5035	0.182	1
C22	0.0445	0.5034	0.2343	1
O23	0.4452	0.0014	0.387	1
O24	0.4213	0.9004	0.0744	1
O25	0.4173	0.1052	0.2358	1
O26	0.4263	0.8995	0.2316	1
O27	0.4219	0.0987	0.0777	1
H28	0.34615	0.79337	0.32458	1
H29	0.34116	0.21056	0.32869	1
H30	0.26567	0.65932	0.33548	1
H31	0.26511	0.34878	0.33687	1
H32	0.1921	0.70385	0.05762	1
H33	0.197	0.30292	0.05583	1
H34	0.28551	0.83176	0.04266	1
H35	0.28713	0.1711	0.04627	1
H36	0.09103	0.72298	0.20669	1
H37	0.30518	0.50494	0.14955	1
H38	0.89163	0.29489	0.26744	1
H39	0.63274	0.99989	0.60555	1
O39s	0.13461	0.09693	0.29481	0.47

O40s	0.12097	0.29006	0.95867	0.91
O41s	0.48988	0.54401	0.90925	1
O42s	0.09509	0.94044	0.92813	1
O43s	0.50727	1.23703	-0.01254	1
O45s	0.95338	0.46272	0.01831	1
O46s	0.88047	0.2369	0.98187	0.83
O47s	0.53934	0.64467	0.5056	1
O49s	0.51868	0.76427	0.34267	0.17
O50s	0.31526	0.94829	0.39917	1
O51s	0.26895	0.98185	0.61693	0.76
O52s	0.52538	0.76562	0.66424	1
Atoms from O39s to O52s in the pores of Fe-TBAPy are represented for the residue electron density of water molecules adsorbed from the surrounding environment during the sample storage and measurement. This is in agreement with the result from the elemental analysis.				

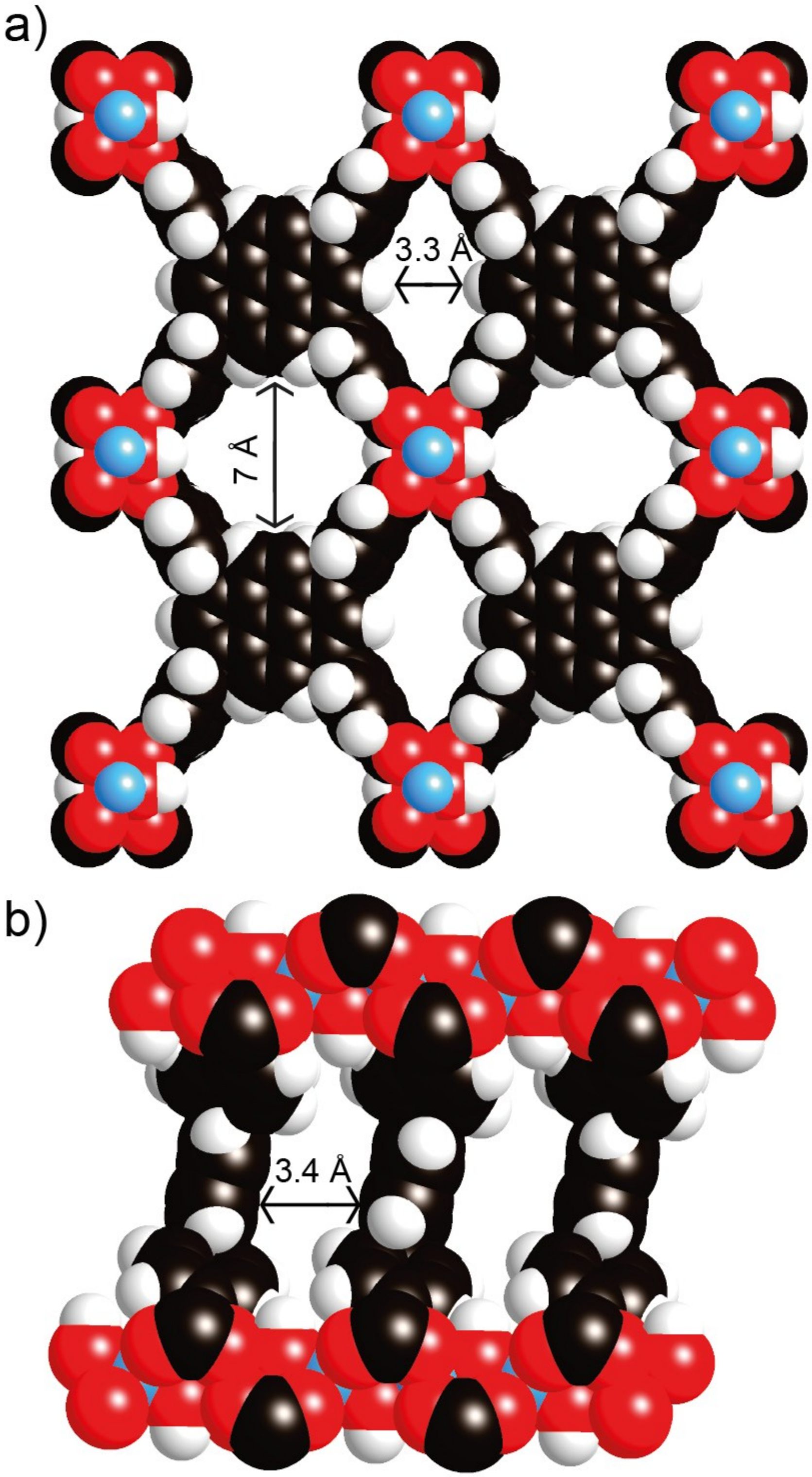

Figure S4. Space-filling model of Fe-TBAPy along Oz axis (a) and the distance between the TBAPy^{4-} linkers (b). Atom colors: Fe, Blue; C, black; O, red; H, white.

Section S5 Fourier Transform Infrared (FT-IR) Analyses

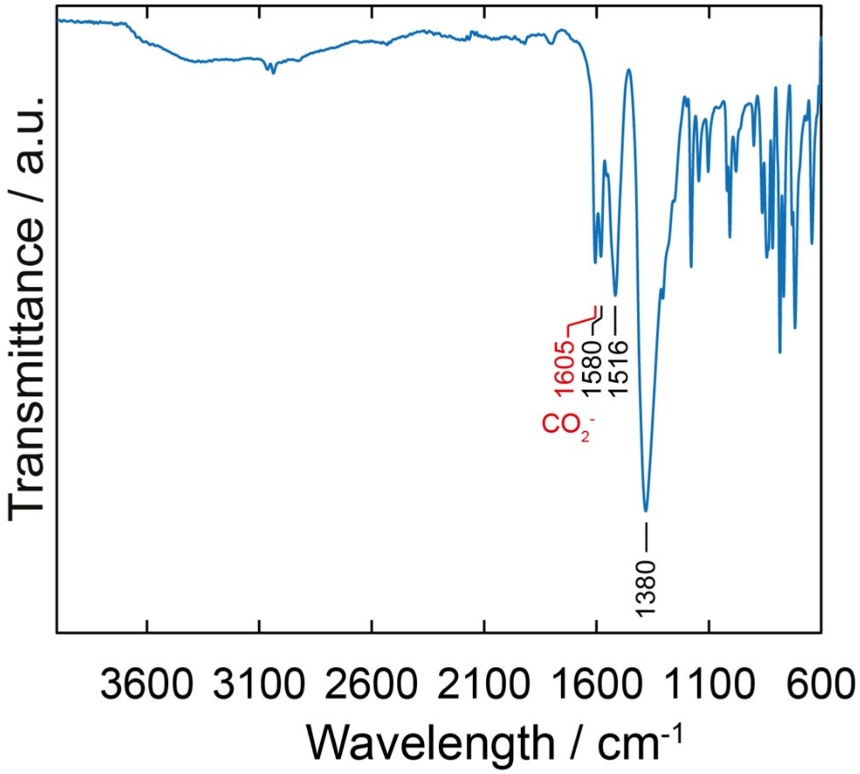

Figure S5. FT-IR spectrum of activated Fe-TBAPy.

Section S6 Thermogravimetric Analyses (TGA)

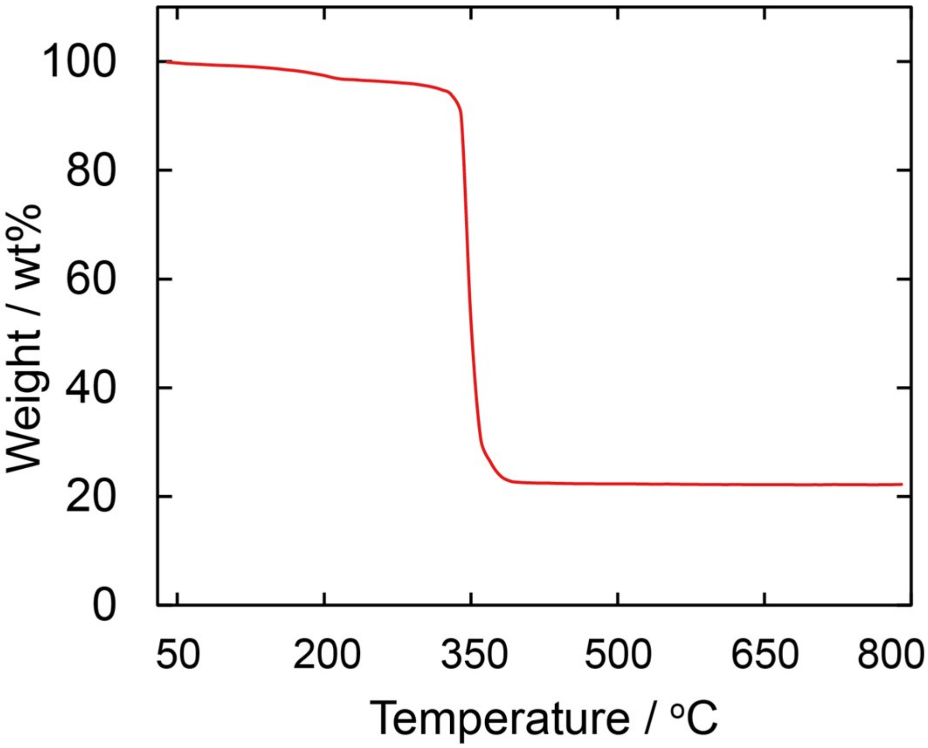

Figure S6. TGA traces of Fe-TBAPy. The amounts of residual metal oxide (attributed to Fe_2O_3) is consistent with the expected values from chemical formula (calcd.: 19.5 wt%; found: 22.2 wt%).

Section S7 77 K N_2 Uptake Measurements and Pore Size Distribution

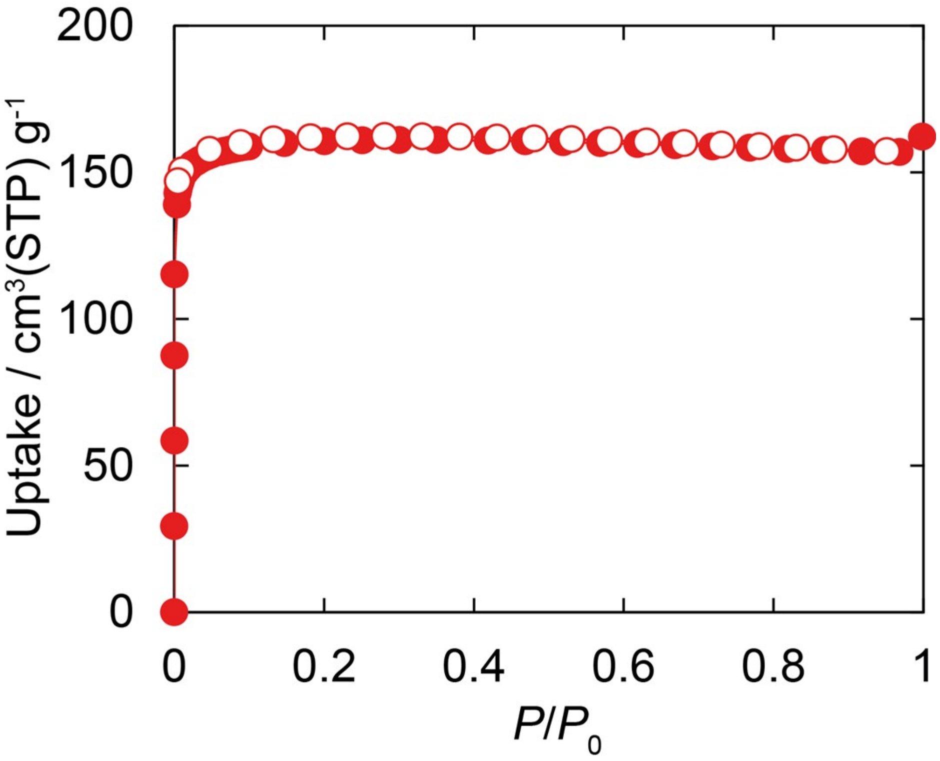

Figure S7. 77 K N_2 isotherm of Fe-TBAPy. The BET (Langmuir) surface area of the sample is calculated to be 650 m^2 g^{-1} (703 m^2 g^{-1}).

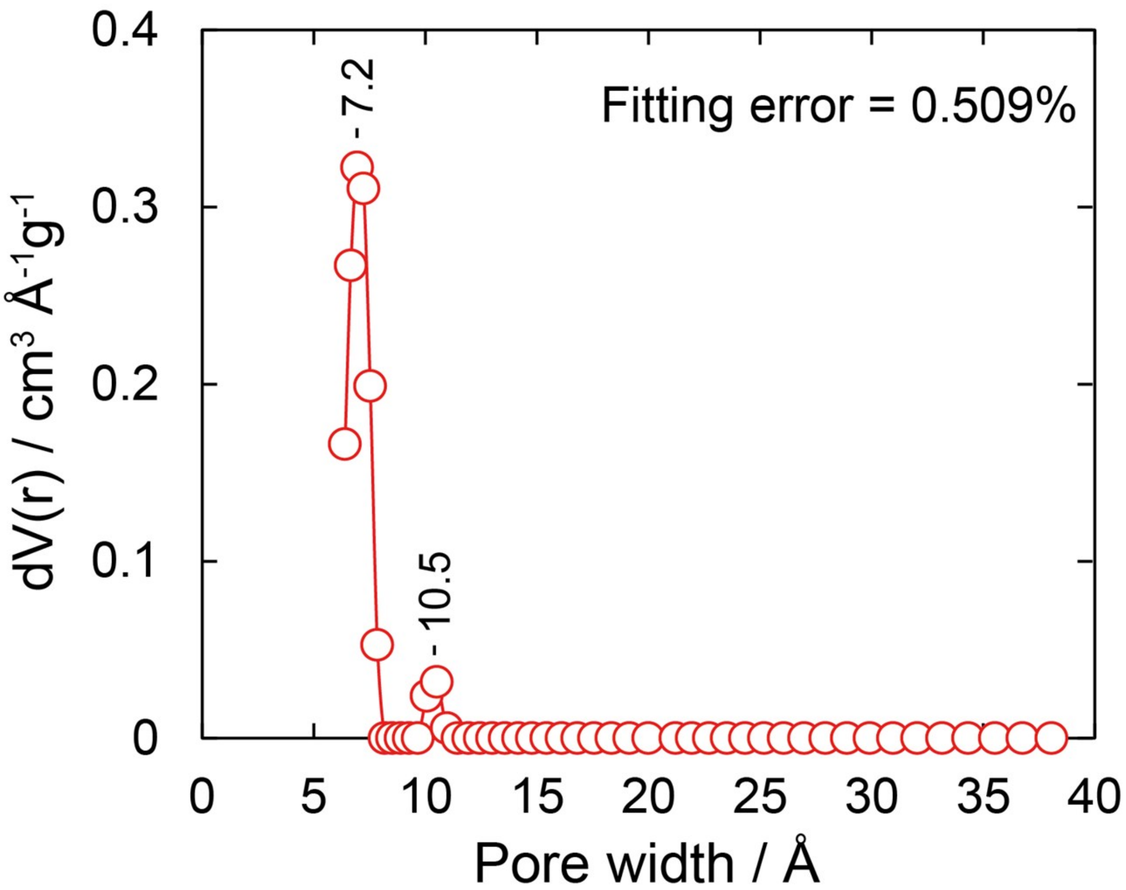

Figure S8. Pore size distribution of Fe-TBAPy N_2 isotherms was analyzed by quenched solid density functional theory (QSDFT) implementing a hybrid kernel for 77 K N_2 adsorption based on a carbon model containing slit/cylinder/sphere pores. The estimated pore width of 7.2 Å corresponds to the hexagonal channel along Oz axis of Fe-TBAPy is found. The peak at 10.5 Å could be attributed to the larger pore formed by the missing linkers.

Section S8 Stability of Fe-TBAPy in Water at Different pH

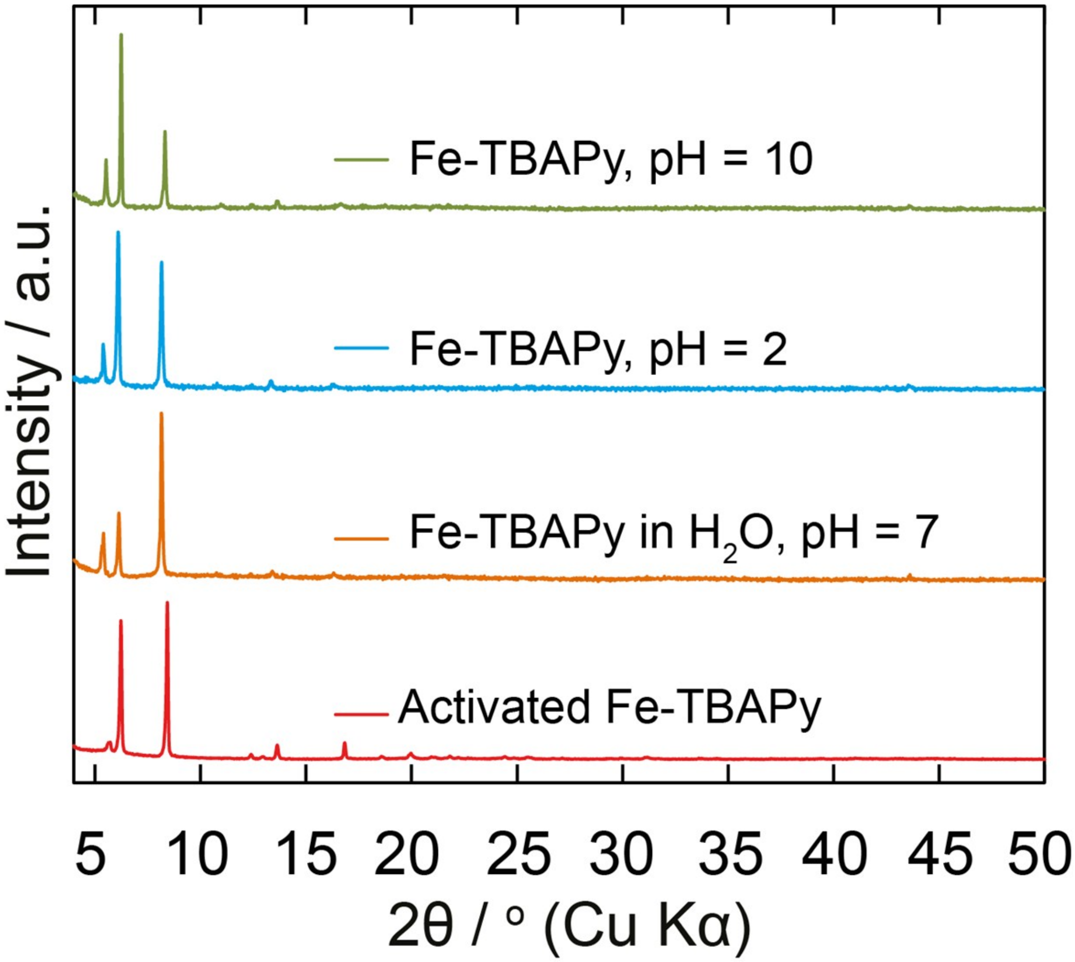

Figure S9. PXRD patterns of Fe-TBAPy after immersion in water at different pH for 5 days. The difference of PXRD patterns of Fe-TBAPy upon immerging in water at various pH are attributed to the structural flexibility of Fe-TBAPy. Further Pawley refinement showed the fitting results with reasonable residual values. The unit cell parameters of Fe-TBAPy were calculated from Pawley fitting with *a* = 14.3414, *b* = 16.1685, *c* = 14.2389 Å, *β*= 84.79 ° for pH = 2 (*Rwp* = 6.73 and *Rp* = 4.95%); *a* = 14.3059, *b* = 16.2956, *c* = 14.0121 Å, *β*= 84.79 ° for pH = 7 (*Rwp* = 6.52 and *Rp* = 4.67%); *a* = 14.1365, *b* = 15.9877, *c* = 13.9914 Å, *β*= 84.80 ° for pH = 10 (*Rwp* = 6.69 and *Rp* = 4.79%) . Activated PXRD pattern of Fe-TBAPy (red) was overlaid as a reference.

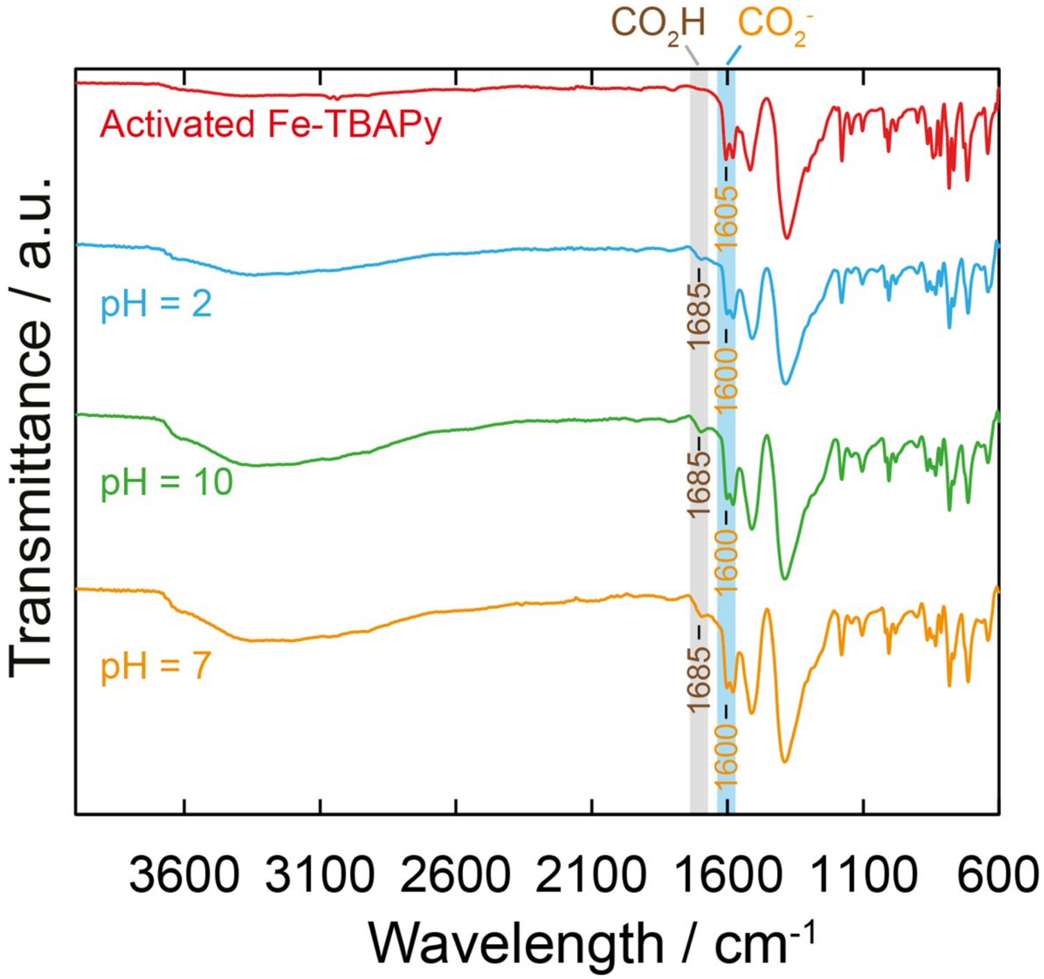

Figure S10. FT-IR spectra of Fe-TBAPy in water at different pH for 5 days. The FT-IR spectra exhibit the characteristic band of the carboxylate group (C=O) appears at 1600 cm^{-1} implying the structural maintenance during the water emerging period.

Section S9 Catalytic Studies for the Hydroxylation of Benzene

Catalysis study. A desired amount of H_2O_2 (30 wt%) was added into a flask pre-charged with acetonitrile/water (2 mL / 2 mL), Fe-TBAPy and benzene (50 μL, 0.56 mmol) (Table S2). Following this, the reaction flask was capped, isothermally heated at the investigated conditions and sampled (~50 μL). The collected sample was then dissolved in ethanol (1.2 mL) with 200 μL toluene solution in ethanol (20 μL / 5 mL) added as the internal standard. The samples were then subjected to GC–FID analysis. The concentration and the phenol yields were calculated using phenol standard curve (Figure S11). The phenol selectivity was calculated using the area-normalization method.[2]

Table S2. Reaction Conditions for Hydroxylation of Benzene.

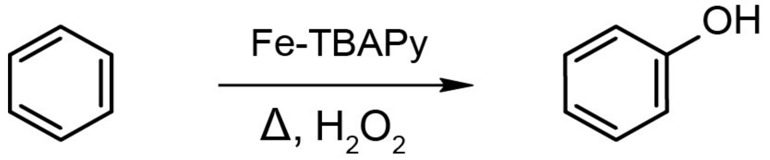

Entry	Catalyst amount (mol%)	H_2O_2 30 wt% (μL)	Temperature (°C)	Time (h)	GC Yield for phenol (%)
1	4.3	100	RT	24	36.0
2			50		40.1
3		400			47.6
4		600			50.26
5	1.0	600	50		43.6
6	1.0	100	70		17.9
7		300			33.9
8		600			57.8
9	**1.0**	**600**	**70**	**33**	**64.5**
10	1.0	600	60		31.9
11			50		40.8
12			40		52.4
13	0.22	600	70	33	35.8
14	0.65				50.5
15	2.1				70.1
16	1.0	300		33	45.6
17		120			25.6
18		60			14.7
19	0	10		33	2.5

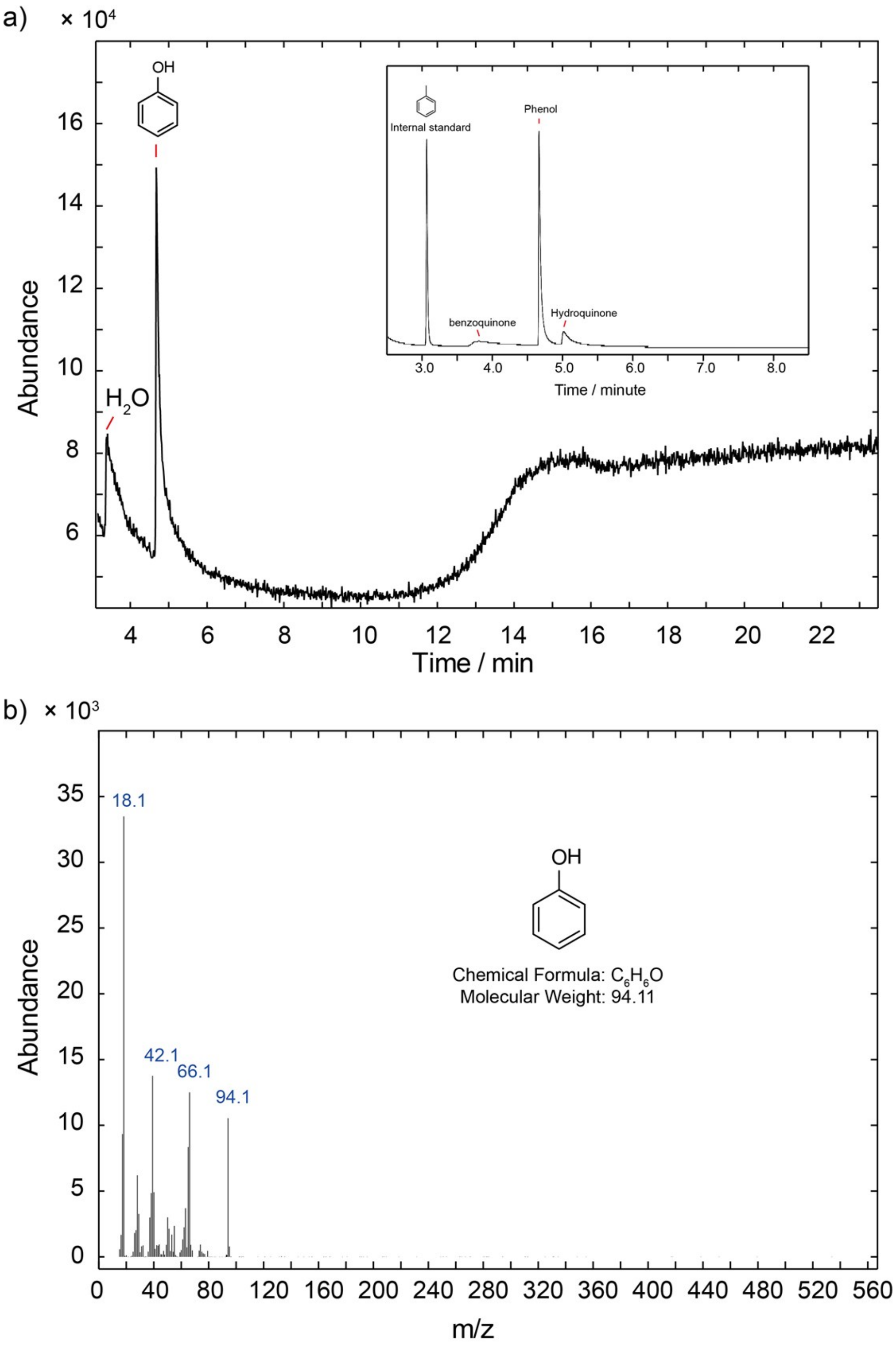

Figure S11. GC analysis: a) Chromatogram and b) MS spectrum of phenol. Benzene cannot be observed in the GC-MS due to the low boiling point. Inset: GC-FID Chromatogram.

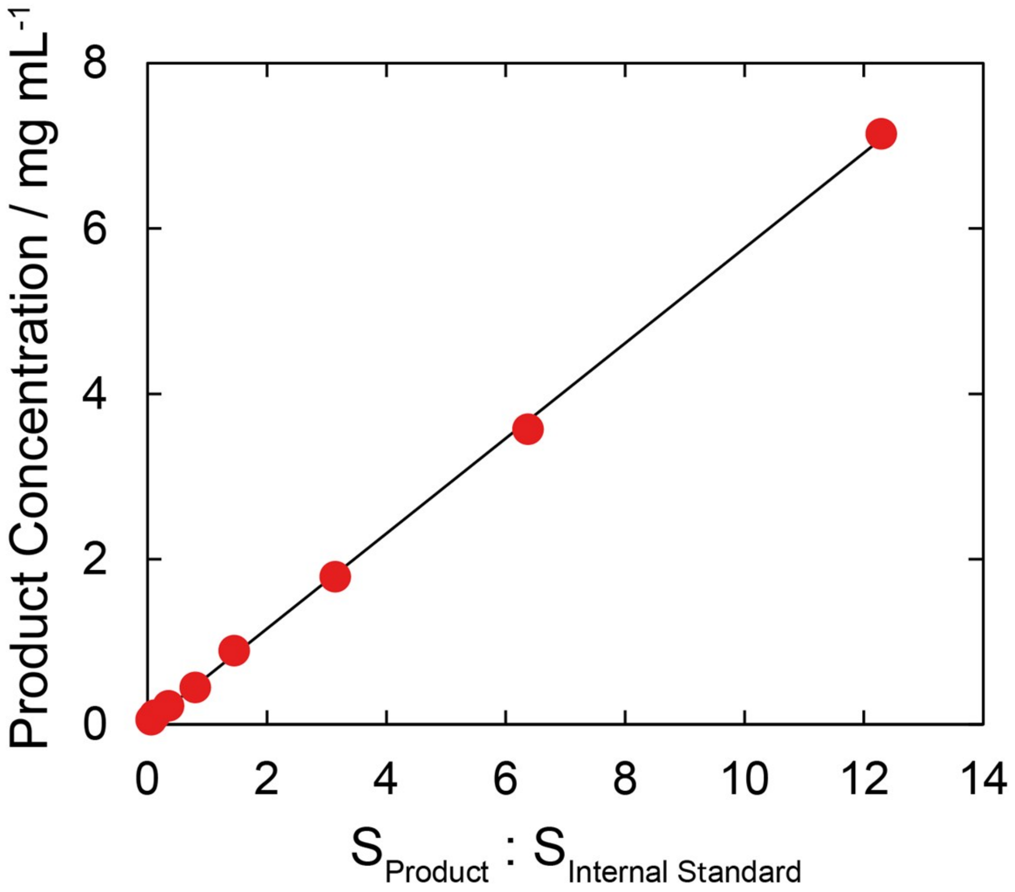

Figure S12. The standard curve for phenol concentration calculation.

Table S3. Heterogeneous Catalysts with High Catalysis Activity for Benzene Hydroxylation.

Catalysts	Temp / °C	Benzene / H_2O_2	Phenol yield	Phenol Selectivity	Refs
V/mp-C_3N_4	60	1 / 1.6	18.0	95.9	2
PMO-1	50	1 / 3	27.4	100	3
$CuCr_2O_4^{RB}$	80	1 / 5	65	95	4
TS-1B	100	10 / 1	8.1	94	5
VPO@GO	60	1 / 3	32.8	100	6
4.2V/NC-600	70	≈ 1 / 3	30	97.2	7
V–Si–ZSM-22	80	1 /1	30.8	99	8
$PMoV_2$/Titania nanotubes	60	3 / 1	27.1	99.1	9
CNT7000	60	1 / 2	5.8	91.5	10
Oxovanadium Schiff base moieties/silica	50	1 / 2	30.8	100	11
TS-1	62	1 / 2.9	29.5	95	12
Ti-HMS			35.1	95	
1%CuAPO-5	60	1 / 2.2	28.0	100	13
CuO/SBA-15	65	1 / 2	19.0	92.4	14
Fc-$MCN_{1.0}$-5	60	9 / 5	14.4	N/A	15
4%Cu/MCM-41	RT	1 / 2	19.7	94	16
Fe-ZSM-5 zeolites	60	N/A	22.9	90	17
Cu_2O-8/dG	RT	1 / 1	19.2	64	18
$PMo_{10}V_2$/pg-C_3N_4	60	1 / 3.5	25.7	99.7	19
CCG	60	1 / 13	18.5	99	20
Cu-SA/HCNS	60	1 / 12.5	83.1	96.7	21
FeOCl	60	1 / 1	43.5	100	22
Fe-TBAPy	RT	1 / 1.6	36^a	100	This work
	50		40^a	94.5	
	70	1 / 10	64.5^b	92.9	
MIL-100	RT	4 / 3	20.1	98%	22
			30.6^c	N/A	
MIL-68	RT	4 / 3	14	90	

^{a}4.3 mol% catalyst; ^{b}1 mol% catalyst; ^{c}Benzene conversion after 24 h.

Section S10 Stability of Fe-TBAPy after Catalytic Recycles

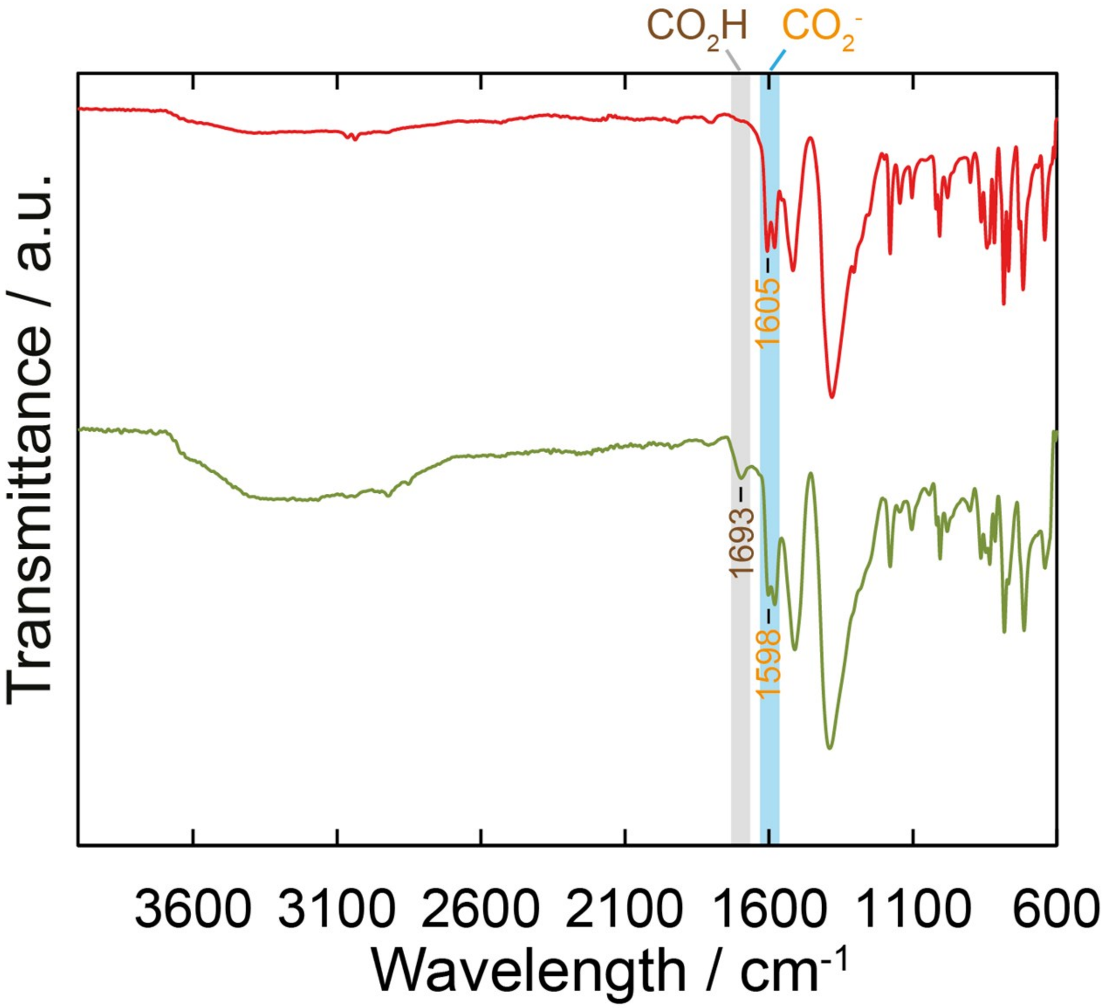

Figure S13. FT-IR spectra of activated Fe-TBAPy (red) and Fe-TBAPy after fifth catalytic cycle (green) for benzene hydroxylation reaction.

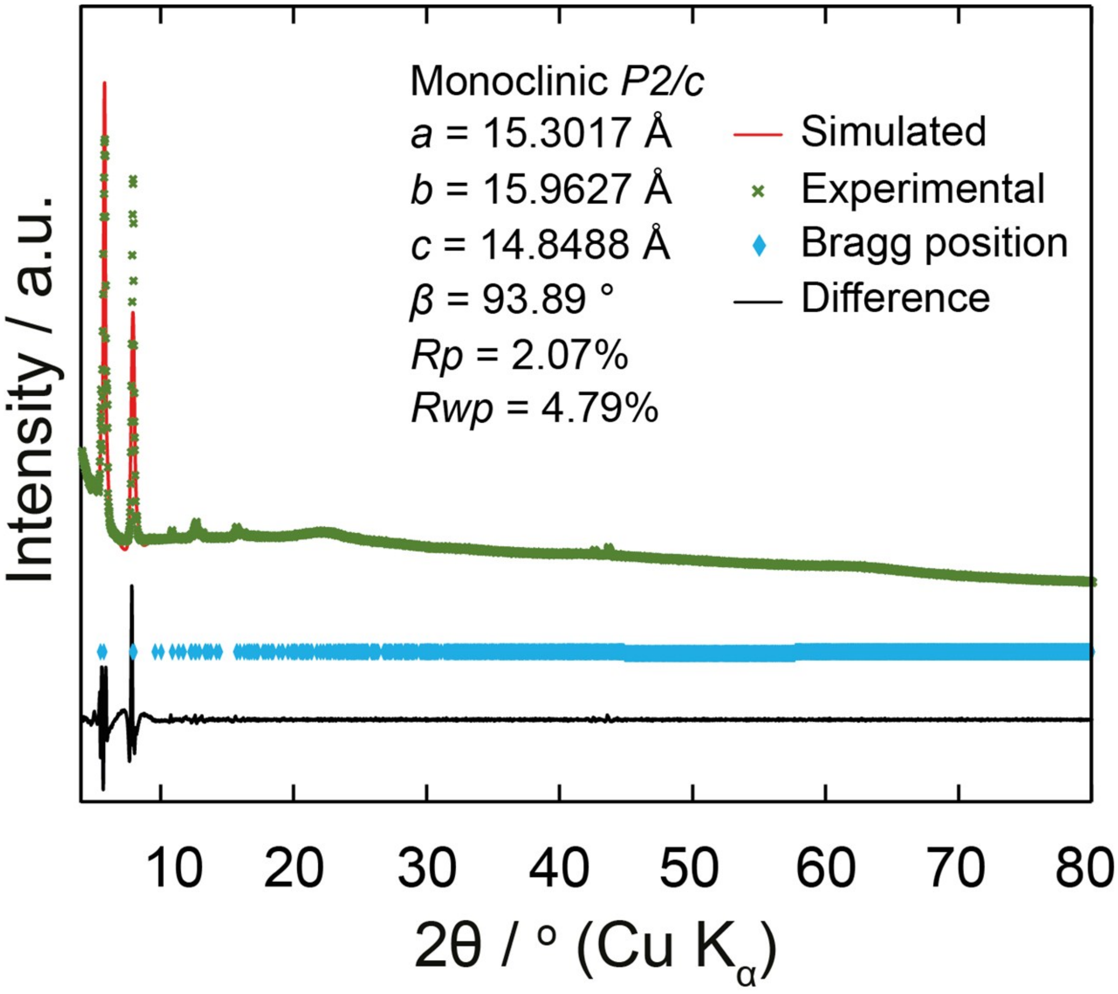

Figure S14. Experimental (green) and Pawley-refined PXRD patterns (red) of recycling Fe-TBAPy. The difference plot (black) and Bragg positions (blue) are provided. The PXRD patterns of recycle Fe-TBAPy showed a slight change of the unit cell parameters comparing with activated Fe-TBAPy.

References

1 K. C. Stylianou, R. Heck, S. Y. Chong, J. Bacsa, J. T. A. Jones, Y. Z. Khimyak, D. Bradshaw and M. J. Rosseinsky, *J. Am. Chem. Soc.*, 2010, **132**, 4119–4130.

2 J. Xu, Q. Jiang, T. Chen, F. Wu and Y. X. Li, *Catal. Sci. Technol.*, 2015, **5**, 1504–1513.

3 P. Borah, X. Ma, K. T. Nguyen and Y. Zhao, *Angew. Chem. Int. Ed.*, 2012, **51**, 7756–7761.

4 S. S. Acharyya, S. Ghosh and R. Bal, *ACS Appl. Mater. Interfaces*, 2014, **6**, 14451–14459.

5 L. Balducci, D. Bianchi, R. Bortolo, R. D'Aloisio, M. Ricci, R. Tassinari and R. Ungarelli, *Angew. Chem. Int. Ed.*, 2003, **42**, 4937–4940.

6 P. Borah, A. Datta, K. T. Nguyen and Y. Zhao, *Green chem.*, 2016, **18**, 397–401.

7 L. Hu, C. Wang, B. Yue, X. Chen and H. He, *RSC Adv.*, 2016, **6**, 87656–87664.

8 Y. Zhou, Z. Ma, J. Tang, N. Yan, Y. Du, S. Xi, K. Wang, W. Zhang, H. Wen and J. Wang, *Nat. Comm.*, 2018, **9**, 2931–2941.

9 H. Wang, C. Wang, M. Zhao, Y. Yang, L. Fang and Y. Wang, *Chem. Eng. Sci.*, 2018, **177**, 399–409.

10 G. Wen, S. Wu, B. Li, C. Dai and D. S. Su, *Angew. Chem. Int. Ed.*, 2015, **54**, 4105–4109.

11 P. K. Khatri, B. Singh, S. L. Jain, B. Sain and A. K. Sinha, *Chem. Commun.*, 2011, **47**, 1610–1612.

12 P. T. Tanev, M. Chibwe and T. J. Pinnavaia, *Nature*, 1994, **368**, 321–323.

13 B. Chou, J. L. Tsai and S. Cheng, *Microporous Mesoporous Mater.*, 2001, **48**, 309–317.

14 A. G. Kong, H. W. Wang, X. Yang, Y. W. Hou and Y. K. Shan, *Microporous Mesoporous Mater.*, 2009, **118**, 348–353.

15 X. Ye, Y. Cui and X. Wang, *ChemSusChem*, 2014, **7**, 738–742.

16 K. M. Parida and D. Rath, *Appl. Catal. A Gen.*, 2007, **321**, 101–108.

17 M. Shahami, K. M. Dooley and D. F. Shantz, *J. Catal.*, 2018, **368**, 354–364.

18 J. He, M. Zhang, A. Primo, H. García and Z. Li, *J. Mater. Chem. A*, 2018, **6**, 19782–19787.

19 H. Wang, M. Zhao, Q. Zhao, Y. Yang, C. Wang and Y. Wang, *Ind. Eng. Chem. Res.*, 2017, **56**, 2711–2721.

20 J.-H. Yang, G. Sun, Y. Gao, H. Zhao, P. Tang, J. Tan, A.-H. Lu and D. Ma, *Energy Environ. Sci.*, 2013, **6**, 793–798.

21 T. Zhang, D. Zhang, X. Han, T. Dong, X. Guo, C. Song, R. Si, W. Liu, Y. Liu and Z. Zhao, *J. Am. Chem. Soc.*, 2018, **140**, 16936–16940.

22 A. E. ElMetwally, G. Eshaq, F. Z. Yehia, A. M. Al-Sabagh, S. Kegnæs, *ACS Catal.*, 2018, 8 (11), 10668–10675.

23 D. Wang, M. Wang and Z. Li, *ACS Catal.*, 2015, **5**, 6852–6857.